AIMS Mathematics, 11(3): 7910–7933.
DOI: 10.3934/math.2026326
Received: 04 February 2026
Revised: 12 March 2026
Accepted: 18 March 2026
Published: 25 March 2026

https://www.aimspress.com/journal/Math

Research article

Analytical dynamics of the Kuralay-II equation: Bifurcation analysis, chaotic behavior, and soliton solution

Alaaeddin Moussa[1,*], Lama Alhakim[1], Abdelnaby S. Saad[1], Yazid Mati[2] and Boubekeur Gasmi[3]

[1] Department of Management Information Systems, College of Business & Economics, Qassim University, P.O. Box 6666, Buraidah, 51452, Saudi Arabia

[2] Department of Operations Management, College of Business & Economics, Qassim University, P.O. Box 6666, Buraidah, 51452, Saudi Arabia

[3] Higher School of Management and Digital Economy, Kolea, Tipaza, Algeria

* **Correspondence:** Email: a.moussa@qu.edu.sa.

Abstract: This paper presents a comprehensive investigation into the complex behavior of the Kuralay-II equation. We begin by analyzing the bifurcation structure and corresponding phase portraits of the equation to gain insight into the underlying dynamical transitions. Next, we examine the chaotic behavior of the governing system through a Lyapunov stability analysis, which provides valuable insights into the sensitivity and stability characteristics of the model. Additionally, we derive several explicit solutions to the equation using an exact analytical method and visualize some of these solutions to highlight their structural properties and dynamical implications. The findings provide a solid framework for future research aimed at understanding the complex behavior of nonlinear systems.

Keywords: Kuralay-II equation; bifurcation analysis; phase portraits; chaos; Lyapunov exponents; exact solutions; nonlinear dynamics; partial differential equations
Mathematics Subject Classification: 34C23, 35C07, 35C08, 34Hxx

1. Introduction

In recent years, many scientists have been studying nonlinear partial differential equations (NPDEs), which can describe a wide range of physical and natural phenomena in our environment [1]. Understanding the dynamic behavior of these phenomena is crucial for improving our quality of life and making informed, accurate, and timely decisions in various fields. By examining NPDEs, we not only enhance our theoretical understanding of their nonlinear behaviors but also gain practical insights that help interpret the solutions in different applications. In physics, (NPDEs) play a crucial role in describing complex dynamical behaviors, such as soliton formation, bifurcation phenomena,

and chaotic dynamics. These equations are widely used across various fields, including optics, plasma physics, fluid dynamics, and quantum mechanics, where they model key processes such as nonlinear wave propagation, fluid instabilities, plasma turbulence, and quantum field interactions. NPDEs also provide essential frameworks for understanding soliton interactions, equilibrium bifurcations, and the emergence of chaos in nonlinear and multiscale physical systems. Significant progress has been made in the solutions of NPDEs using a variety of analytical and numerical methods. Among these techniques, several have proven to be particularly effective and reliable. Notable methods include the Cham method [2], the improved Cham method [3], the $\coth_a(\xi)$ expansion method [4], the $\tanh(\xi)$ expansion method [5], and the improved modified extended tanh function technique [6]. Other important approaches are the new $(\acute{G}/G)$ expansion technique [7], the generalized $\exp(-\phi(\xi))$ expansion method [8], the double auxiliary equation method [9], the generalized double auxiliary equation method [10], the modified extended direct algebraic method [11], and the modified extended mapping method [12]. Additionally, techniques such as the generalized Kudryashov method [13], the Hirota bilinear form [14], the modified Sardar subequation method [15], and the modified extended direct algebraic method [16] have also made significant contributions. Finally, Darboux transformations and related analytical techniques [19], similarity transformations [17], and the radial basis functions technique [18] are also important tools in this area of research.

This study focuses on the Kuralay-II equation. The objective is to investigate the bifurcation, chaotic behavior, and soliton solutions of this equation through analytical methods. The Kuralay-II equation is defined in Eq (1.1).

$$\begin{cases} i\Xi_t - \Xi_{xt} - \Xi\Lambda = 0, \\ iR_t + R_{xt} + \Xi\Lambda = 0, \\ \Lambda_x + 2k^2(R\Xi)_t = 0, \end{cases} \tag{1.1}$$

where $\Xi(x,t)$ and $R(x,t)$ denote unknown complex functions, and $\Lambda(x,t)$ is referred to as the real function, with k being a standard constant.

The Kuralay-II equation is essential in various fields, such as engineering, mechanics, quantum mechanics, and other areas of nonlinear science. It serves as a versatile model for describing complex nonlinear phenomena and exhibits rich dynamical behavior such as equilibrium bifurcations, sensitivity to perturbations, and the coexistence of solitary, periodic, and chaotic wave regimes. Several exact methods have been proposed to solve this equation. In [20], the authors employed the extended auxiliary equation method along with the modified expansion method to derive solutions and analyze modulation instability. The authors in [21] utilized the improved F-expansion method, and the Hirota bilinear method was applied in [22, 23]. In [24], both the extended hyperbolic functions method and the improved F-expansion method were used. Furthermore, [25] employed the $\exp_a$ function, the extended sine-Gordon equation expansion scheme, and generalized Kudryashov schemes. The Jacobi elliptic function expansion method was implemented in [26], and the new auxiliary equation method was applied in [27].

Although significant progress has been made in solving the Kuralay-II equation, several challenges still require further investigation. In particular, additional families of solutions need to be derived to improve the understanding of the complex dynamical behaviors associated with the Kuralay-II equation. Moreover, it is important to examine how its integrable soliton structures transition into chaotic states when subjected to external periodic forcing. The precise bifurcation mechanisms that lead to temporal complexity also remain largely unexplored. This work aims to address these

gaps by conducting a systematic dynamical analysis, including global bifurcation mapping and the identification of routes to chaos. Additionally, the study proposes a new approach to find novel explicit solutions to the equation. The remainder of this paper is organized as follows. Section 2 explores the application of bifurcation theory to identify equilibrium points within the associated Hamiltonian system and analyze their stability characteristics. Section 3 investigates the chaotic dynamics exhibited by the system. Section 4 introduces a novel approach to derive new analytical solutions for the Kuralay-II equation. Section 5 presents 3D graphical representations that illustrate the real and absolute parts of some selected solutions. Section 6 is devoted to the physical analysis and comparative study of the obtained wave solutions. Finally, Section 7 summarizes the main findings and outlines potential directions for future research.

2. Bifurcation and phase portraits

A thorough understanding of a system's intrinsic dynamics is crucial for accurately describing its long-term behavior across different initial conditions. Soliton behaviors and their dependence on system parameters play an important role in explaining nonlinear wave phenomena and supporting applications in optics, plasma physics, and fluid dynamics. In contrast to Gaussian pulse forcing, our model focuses on periodic excitation and investigates its role in triggering transitions to chaotic dynamics [28].

In this section, we apply bifurcation theory [29] to analyze the complex dynamics of the Kuralay-II equation and construct detailed phase portraits.

Setting $k = 1$ and $R = \varepsilon\,\overline{\Xi}$, where $(\varepsilon = \pm 1)$, Eq (1.1) becomes as follows:

$$\begin{cases} i\Xi_t - \Xi_{xt} - \Xi\Lambda = 0, \\ \Lambda_x - 2\varepsilon(|\Xi|^2)_t = 0. \end{cases} \tag{2.1}$$

Using the traveling wave transformation given in (2.2),

$$\begin{cases} \Xi(x,t) = \Theta(\xi)e^{i\kappa}, & \kappa = m_1 x + m_2 t, \\ \Lambda(x,t) = \frac{2\varepsilon m_2}{(1-m_1)}\Theta^2(\xi) + c, & c = \frac{c_1 m_2}{k_1(1-m_1)}, k_1 \neq 0, \\ \xi = \frac{k_1(1-m_1)}{m_2}x + k_1 t, & m_1 \notin \{0,1\}, m_2 \neq 0, \end{cases} \tag{2.2}$$

where m_1, m_2, c_1, and k_1 are real constants, Eq (2.1) is transformed into the following form:

$$\Theta'' + \frac{m_2(m_2(m_1-1)-c)}{k_1^2(m_1-1)}\Theta + \frac{2\varepsilon m_2^2}{k_1^2(m_1-1)^2}\Theta^3 = 0. \tag{2.3}$$

The dynamical system derived from Eq (2.3) can be expressed as follows:

$$\begin{cases} \frac{d\Theta(\xi)}{d\xi} = \Phi(\xi), \\ \frac{d\Phi(\xi)}{d\xi} = -A\Theta(\xi) - B\Theta^3(\xi), \end{cases} \tag{2.4}$$

where

$$A = \frac{m_2(m_2(m_1-1)-c)}{k_1^2(m_1-1)}, \quad B = \frac{2\varepsilon m_2^2}{k_1^2(m_1-1)^2}.$$

The parameters A and B play a fundamental role in determining the dynamical behavior of the reduced system. Specifically, A governs the linear stability of the wave amplitude and acts as an effective linear restoring coefficient, arising from the balance between the wave propagation parameters introduced through the traveling wave transformation. In contrast, B characterizes the strength of the nonlinear interactions within the system. Variations in the signs and magnitudes of A and B significantly influence the qualitative structure of the phase portraits and can lead to different wave patterns, including periodic oscillations, solitary waves, and homoclinic trajectories.

The first integral is given by Eq (2.5):

$$H(\Theta, \Phi) = 2\Phi^2 + 2A\Theta^2 + B\Theta^4 = h. \tag{2.5}$$

The equilibrium points of the system are determined by solving the equations $d\Theta/d\xi = 0$ and $d\Phi/d\xi = 0$. When $AB > 0$, there exists a single equilibrium point $E_1(0,0)$. In contrast, when $AB < 0$, three equilibrium points emerge: $E_1(0,0)$, $E_2(\sqrt{-A/B}, 0)$, and $E_3(-\sqrt{-A/B}, 0)$. The determinant of the Jacobian matrix at an equilibrium point (Θ_e, Φ_e) is given by

$$J(\Theta_e, \Phi_e) = \begin{vmatrix} 0 & 1 \\ -A - 3B\Theta_e^2 & 0 \end{vmatrix} = A + 3B\Theta_e^2.$$

Moreover, the trace of the matrix at each equilibrium point satisfies $\text{Trace}(E_k) = 0, k = 1, 2, 3$. Building on the previous points, we now examine all possible bifurcation cases of the dynamical system (2.4) as follows:

Case 1: When $A > 0$ and $B > 0$, the system admits a single equilibrium point at $E_1(0,0)$. This point is identified as a center because $J(E_1) = A > 0$ and $\text{Trace}(E_1) = 0$. The phase portrait shows closed orbits, which correspond to periodic wave solutions of Eq (2.3).

Case 2: When $A < 0$ and $B < 0$, the system has a single equilibrium point at $E_1(0,0)$, which is classified as a saddle point because $J(E_1) = A < 0$. The phase trajectories create homoclinic orbits around this saddle point, indicating the existence of solitary wave solutions for Eq (2.3).

Case 3: When $A > 0$ and $B < 0$, the system exhibits three equilibrium points $E_1(0,0)$, $E_2\left(\sqrt{-A/B}, 0\right)$, and $E_3\left(-\sqrt{-A/B}, 0\right)$. The point $E_1(0,0)$ behaves as a center because $J(E_1) = A > 0$ and $\text{Trace}(E_1) = 0$, and the points E_2 and E_3 are saddle points as, $J(E_{2,3}) = -2A < 0$. Accordingly, periodic wave solutions are associated with closed orbits surrounding the center, whereas solitary wave solutions correspond to homoclinic orbits around the saddle points.

Case 4: When $A < 0$ and $B > 0$, the system has three equilibrium points: $E_1(0,0)$, $E_2\left(\sqrt{-A/B}, 0\right)$, and $E_3\left(-\sqrt{-A/B}, 0\right)$. The point $E_1(0,0)$ is a saddle point given that $J(E_1) = A < 0$. The points E_2 and E_3 act as centers because $J(E_{2,3}) = -2A > 0$ and $\text{Trace}(E_{2,3}) = 0$. Thus, solitary wave solutions are associated with the saddle point, whereas periodic wave solutions arise around the centers. Figures 1 and 2 present graphical representations of the dynamical behavior of the system for the four aforementioned cases, using selected values of A and B. Figure 1 shows the bifurcation of the phase portraits for Cases 1 and 2, whereas Figure 2 corresponds to Cases 3 and 4.

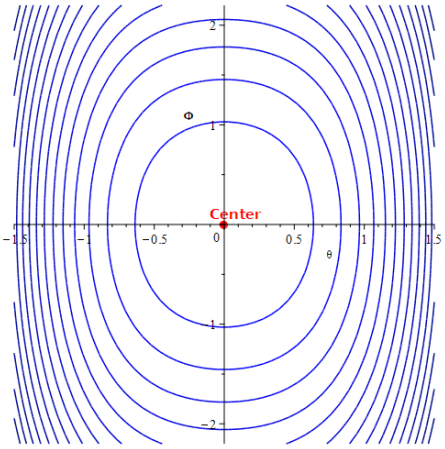

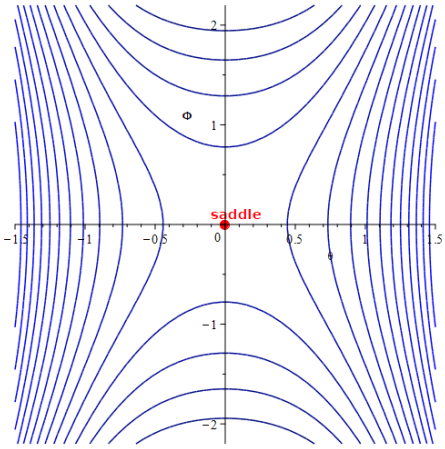

Figure 1. The left (resp. right) shows the bifurcation of phase portraits for system (2.4) with $A = 2$ and $B = 3$ (resp. $A = -2$ and $B = -3$).

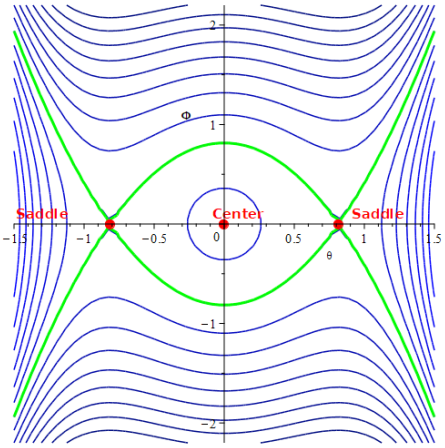

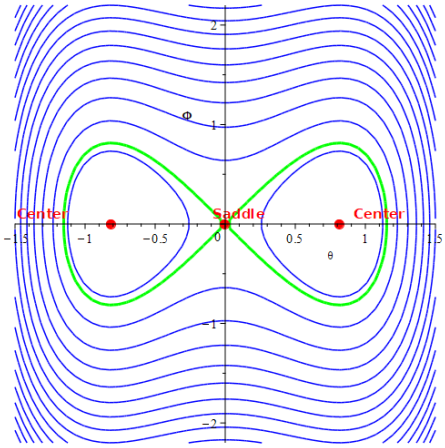

Figure 2. The left (resp. right) shows the bifurcation of phase portraits for system (2.4) with $A = 2$ and $B = -3$ (resp. $A = -2$ and $B = 3$).

3. Chaotic behavior and Lyapunov stability analysis

Some studies on chaotic behavior have investigated the interaction of solitary waves with external forcing using bifurcation analysis [31], whereas other works have examined nonlinear dynamical responses and transition mechanisms in similar forced systems [32]. In contrast to the chaotic transitions induced by Gaussian pulse forcing reported in [31], the analysis of this section demonstrates that continuous periodic excitation leads to a distinct period-doubling route to chaos, resulting in a different evolution of the Lyapunov spectra. The aim is to identify transitions among stable, periodic, and chaotic regimes while offering insights into the bifurcation structure and the overall dynamics of the system.

3.1. Chaotic behavior

We introduce a periodic perturbation term $a\cos(b\xi)$, where a represents the perturbation amplitude and b denotes its frequency. Such perturbations are commonly observed in real-world physical systems [33]. Building on this, we investigate the presence of chaos by analyzing 2D and 3D phase portraits. Accordingly, the perturbed system takes the following form:

$$\begin{cases} \frac{d\Theta(\xi)}{d\xi} = \Phi(\xi), \\ \\ \frac{d\Phi(\xi)}{d\xi} = -A\Theta(\xi) - B\Theta^3(\xi) + a\cos(b\xi), \end{cases} \tag{3.1}$$

where

$$A = \frac{m_2(m_2(m_1-1)-c)}{k_1^2(m_1-1)}, \quad B = \frac{2\varepsilon m_2^2}{k_1^2(m_1-1)^2}.$$

Figure 3 analyzes the unperturbed scenario by setting $a = 0$, corresponding to the original system described in Eq (2.4). The figure presents phase portraits for $A = 2$, $B = 3$, and initial conditions $\Theta(0) = 0.02$, $\Phi(0) = 0.03$, illustrating the onset of chaotic behavior in the nonlinear dynamical system (3.1).

Figure 4 demonstrates that the system retains quasi-periodic behavior as the perturbation amplitude a increases from 0 to 0.001, with $b = 0.002$ and other parameters unchanged. This indicates that the system is largely insensitive to small perturbations, as its trajectories closely resemble those of the unperturbed case. Therefore, the system displays robustness and dynamical stability under weak external disturbances.

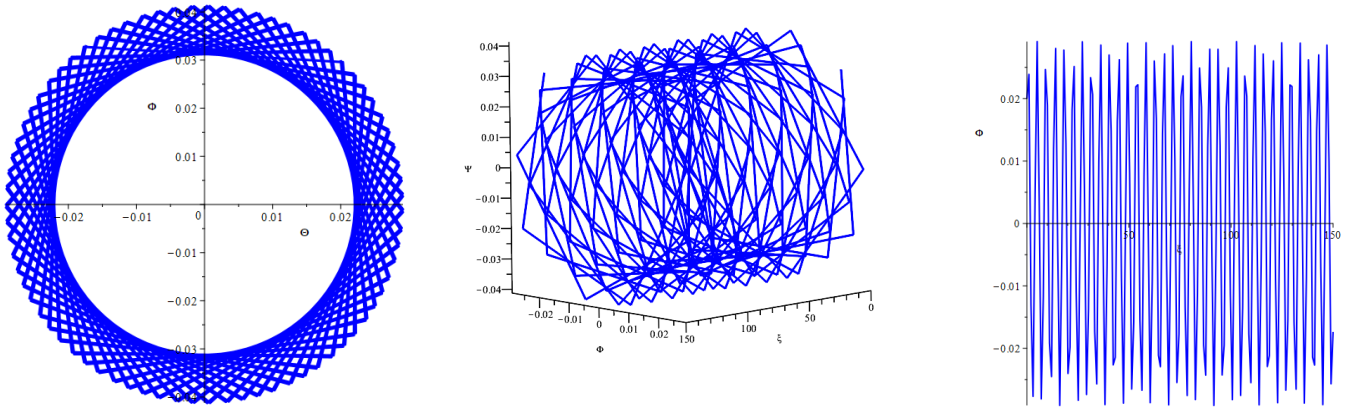

(a) 2D phase portraits (b) 3D phase portraits (c) Time series

Figure 3. The behavior of the dynamical system (3.1) without a perturbation term.

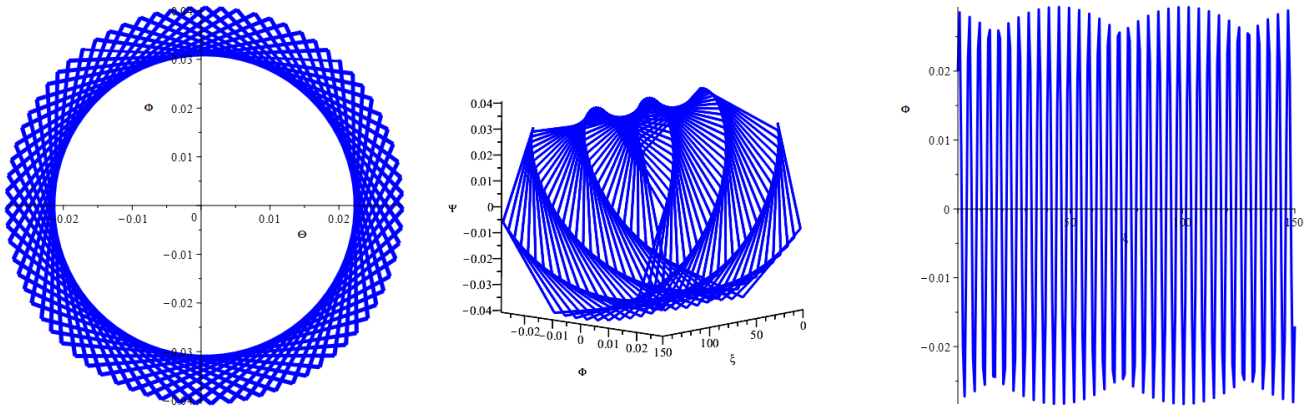

(a) 2D phase portraits (b) 3D phase portraits (c) Time series

Figure 4. The behavior of the dynamical system (3.1) with a perturbation term $0.001\cos(0.002\xi)$.

Figure 5 illustrates a transition in the dynamical system as the perturbation amplitude a increases from 0.001 to 0.01 and the frequency parameter b increases from 0.002 to 0.02. These parameter changes cause a loss of stability and the onset of chaotic dynamics, as evidenced by the 2D and 3D phase portraits. The corresponding time series displays a shift from regular to chaotic patterns.

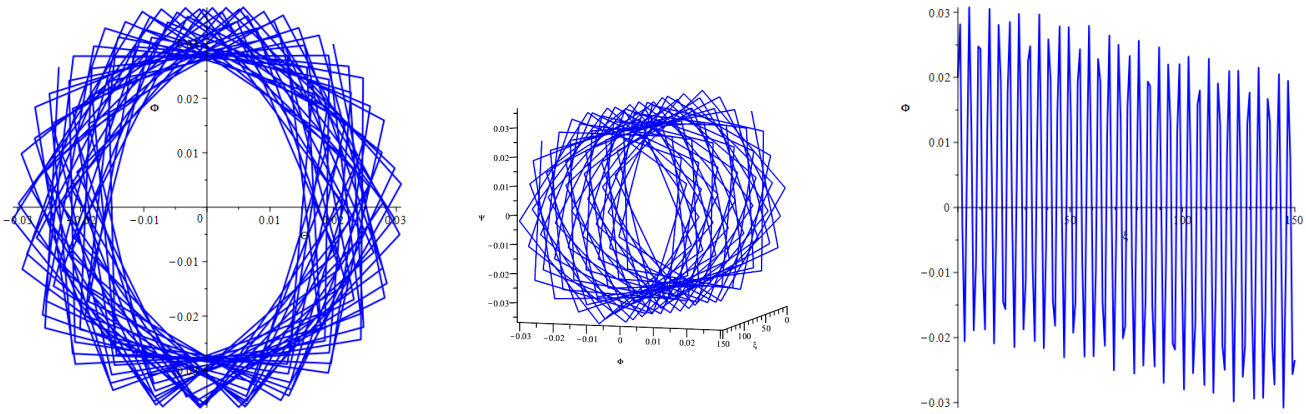

(a) 2D phase portraits (b) 3D phase portraits (c) Time series

Figure 5. The behavior of the dynamical system (3.1) with a perturbation term $0.01\cos(0.02\xi)$.

Figure 6 demonstrates that increasing the perturbation amplitude from 0.01 to 0.1 and the frequency parameter from 0.02 to 0.2 produces irregular, nonperiodic trajectories. This change indicates a complete loss of stability. Both the 2D and 3D phase portraits confirm the presence of fully developed chaotic behavior. The corresponding time series corroborates this result by showing a transition from order to chaos. These results indicate that the system operates in a fully chaotic regime under intensified perturbations.

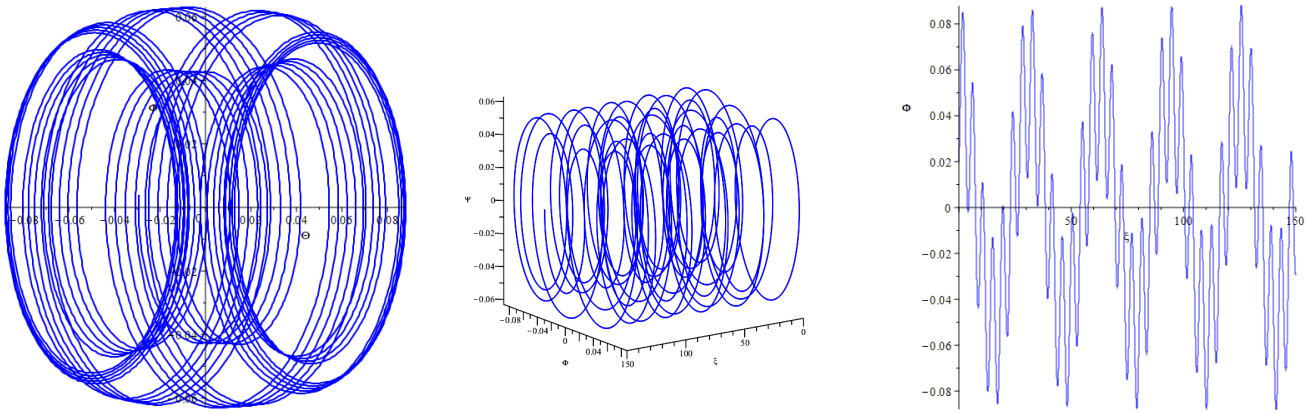

(a) 2D phase portraits (b) 3D phase portraits (c) Time series

Figure 6. The behavior of the dynamical system (3.1) with a perturbation term $0.1\cos(0.2\xi)$.

In summary, numerical simulations indicate that periodic perturbations substantially modify the dynamical behavior of the system. The system transitions from stable to quasi-periodic and ultimately to chaotic motion as perturbation strength increases. These results confirm the presence of chaos within specific parameter ranges and demonstrate that minor parameter variations can induce significant qualitative changes in the system dynamics.

3.2. Lyapunov stability analysis

Before analyzing the chaotic characteristics of the perturbed system, it is essential to establish a baseline for the unperturbed case ($a = 0$). In this scenario, the system (3.1) is conservative and exhibits only periodic behaviors, as indicated by a vanishing maximum Lyapunov exponent ($\lambda_{max} \approx 0$). The transition to chaotic dynamics is strictly contingent upon the introduction of the periodic forcing term ($a > 0$), which breaks the integrability of the system and leads to a positive maximum Lyapunov exponent.

Lyapunov exponents measure the average exponential rates at which nearby trajectories in a nonlinear dynamical system diverge or converge. The exponents are determined from the real parts of the eigenvalues of the system's differential equations and provide essential information regarding system stability. Lyapunov exponents are instrumental in identifying transitions among periodic, period-doubling, and chaotic regimes during bifurcation analysis. A positive largest Lyapunov exponent indicates chaotic dynamics, whereas a negative value signifies stable behavior.

The Lyapunov exponents for the dynamical system defined in Eq (3.1) were numerically computed using specialized routines in Mathematica with high-precision settings to ensure the convergence of the spectral exponents. Figure 7 presents the convergence of these exponents when a weak perturbation term of $0.001\cos(0.002\xi)$ is applied. The calculated exponents are $\lambda_1 = 0.0109023180$, $\lambda_2 = -0.0109023180$, and $\lambda_3 = 0$, represented by blue, orange, and green lines, respectively. These results demonstrate that the system maintains a stable periodic or quasi-periodic motion for initial conditions $\Theta(0) = 0.02$ and $\Phi(0) = 0.03$ under weak perturbations. Figure 8 depicts the convergence of Lyapunov exponents with a stronger perturbation term of $0.1\cos(0.2\xi)$. Under these conditions, the exponents are $\lambda_1 = 0.0248963470$ (blue line), $\lambda_2 = -0.0248963470$ (orange line), and $\lambda_3 = 0$

(green line).

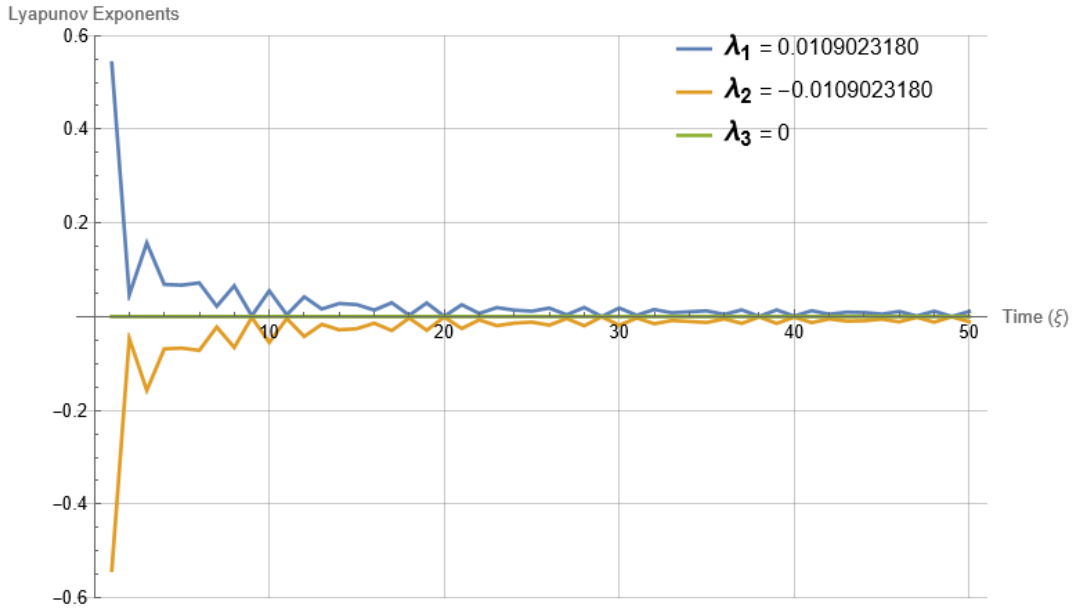

Figure 7. Convergence of Lyapunov exponents of the dynamical system (3.1) with a weak perturbation term $0.001\cos(0.002\xi)$.

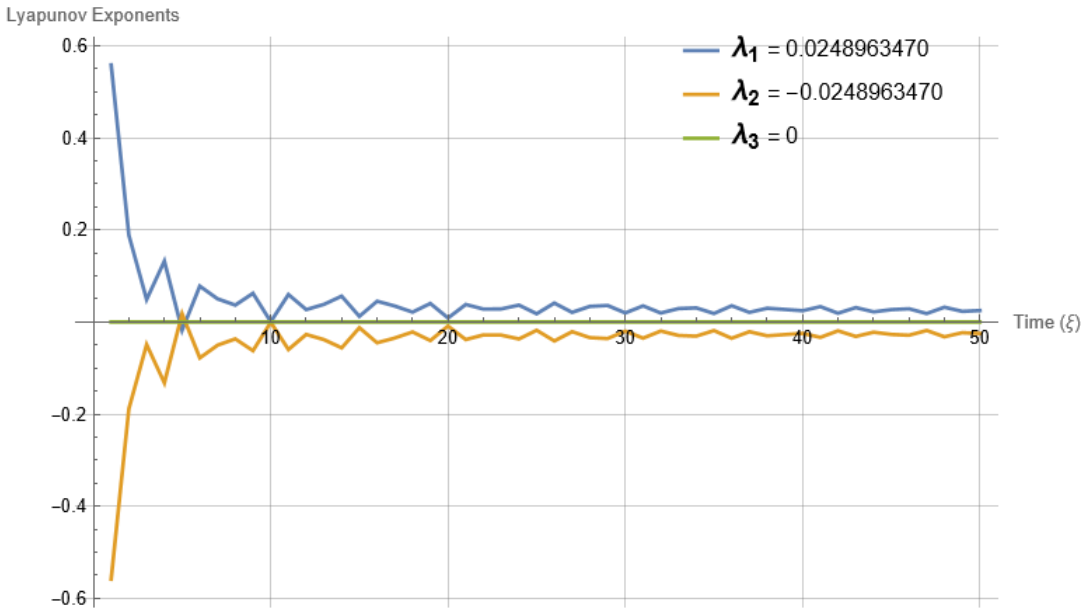

Figure 8. Convergence of Lyapunov exponents of the dynamical system (3.1) with a stronger perturbation term $0.1\cos(0.2\xi)$.

To ensure the reproducibility of the reported Lyapunov exponents, numerical integration was performed using the Runge–Kutta–Fehlberg algorithm. This computation involved the simultaneous integration of the dynamical system described in Eq (3.1) and its associated variational equations. We employed a step size of $\Delta t = 0.01$ over a sufficiently long time interval ($T = 50$) to achieve

stable convergence. The relative and absolute error tolerances were set to 10^{-7} and 10^{-8}, respectively. Additionally, the Gram–Schmidt reorthonormalization procedure was applied at each integration step to prevent the alignment of tangent vectors and accurately capture the spectrum of exponents.

3.3. Global bifurcation analysis and the transition to chaos

To provide a deeper understanding of the dynamical transitions within the Kuralay-II system (3.1), a detailed numerical bifurcation analysis was conducted. Figure 9 illustrates the bifurcation diagram of the state variable θ as a function of the forcing frequency b, which serves as the primary control parameter. The diagram reveals a classical period-doubling route to chaos, a fundamental mechanism in nonautonomous nonlinear oscillators.

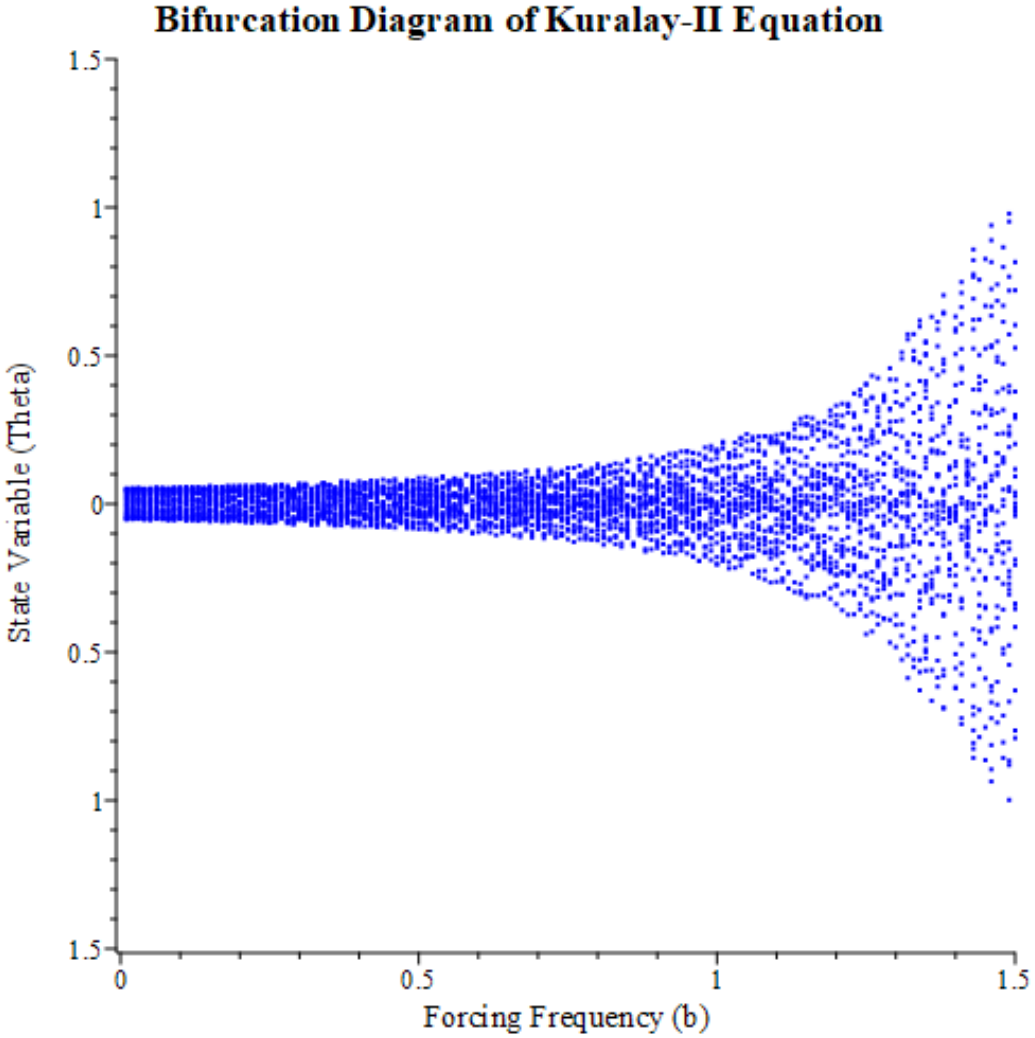

Figure 9. Bifurcation diagram of the dynamical system (3.1) for the state variable θ versus the forcing frequency b, with $A = 2, B = 3$, and $a = 0.1$. The plot illustrates the transition from stable periodic motion to a chaotic regime through a clear period-doubling cascade.

Initially, for lower frequency regimes, the system's attractor is a stable limit cycle of period-1. As b varies, the system undergoes a sequence of period-doubling cascades (flip bifurcations), where the

stability of the period-n orbit is lost in favor of a stable period-$2n$ orbit. This hierarchical branching process continues until the onset of a chaotic attractor is observed, where the trajectories become nonperiodic and highly sensitive to initial conditions. The emergence of these chaotic bands in the bifurcation diagram is perfectly consistent with the regions of positive Lyapunov exponents ($\lambda > 0$) reported in the previous section. This synergy between qualitative bifurcation mapping and quantitative Lyapunov analysis provides a solid validation of the complex nonlinear phenomena inherent in the Kuralay-II equation.

4. Finding exact solutions to the Kuralay-II equation

To solve the Kuralay-II equation, we need to investigate the solutions of Eq (2.3). For this purpose, we consider the following auxiliary differential equation:

$$\left(\frac{d}{d\xi}h(\xi)\right)^2 = \delta_1 h^4(\xi) + \delta_2 h^2(\xi) + \delta_0. \tag{4.1}$$

Equation (4.1) admits several exact solutions, described in the following: *Family 1*: When $\delta_2^2 - 4\delta_0\delta_1 > 0$ and $\delta_0\delta_1 \neq 0$,

$$h(\xi) = \pm \frac{\delta_0 \sqrt{2}\, \mathrm{sn}\left(\frac{\sqrt{2\sqrt{\delta_2^2-4\delta_0\delta_1}-2\delta_2}}{2}(\xi+\xi_0), \frac{\sqrt{-2\left(\delta_2\sqrt{\delta_2^2-4\delta_0\delta_1}+2\delta_0\delta_1-\delta_2^2\right)\delta_0\delta_1}}{\delta_2\sqrt{\delta_2^2-4\delta_0\delta_1}+2\delta_0\delta_1-\delta_2^2} \right)}{\sqrt{\delta_0\left(\sqrt{\delta_2^2-4\delta_0\delta_1}-\delta_2\right)}}, \quad \xi_0 \in \mathbb{R}. \tag{4.2}$$

Family 2: When $\delta_2^2 - 4\delta_0\delta_1 = 0$, $\delta_1 > 0$, and $\delta_2 < 0$,

$$h(\xi) = \pm\sqrt{-\frac{\delta_2}{2\delta_1}}\tanh\left(\sqrt{-\frac{\delta_2}{2}}(\xi+\xi_0)\right), \quad \xi_0 \in \mathbb{R}. \tag{4.3}$$

$$h(\xi) = \pm\sqrt{-\frac{\delta_2}{2\delta_1}}\coth\left(\sqrt{-\frac{\delta_2}{2}}(\xi+\xi_0)\right), \quad \xi_0 \in \mathbb{R}. \tag{4.4}$$

Family 3: When $\delta_2^2 - 4\delta_0\delta_1 = 0$, $\delta_1 > 0$, and $\delta_2 > 0$,

$$h(\xi) = \pm\sqrt{\frac{\delta_2}{2\delta_1}}\tan\left(\sqrt{\frac{\delta_2}{2}}(\xi+\xi_0)\right), \quad \xi_0 \in \mathbb{R}. \tag{4.5}$$

$$h(\xi) = \pm\sqrt{\frac{\delta_2}{2\delta_1}}\cot\left(\sqrt{\frac{\delta_2}{2}}(\xi+\xi_0)\right), \quad \xi_0 \in \mathbb{R}. \tag{4.6}$$

Family 4: When $\delta_0 > 0$, $\delta_1 = 0$, and $\delta_2 < 0$,

$$h(\xi) = \pm\sqrt{-\frac{\delta_0}{\delta_2}}\sin\left(\sqrt{-\delta_2}(\xi+\xi_0)\right), \quad \xi_0 \in \mathbb{R}. \tag{4.7}$$

$$h(\xi) = \pm\sqrt{-\frac{\delta_0}{\delta_2}}\,\cos\Big(\sqrt{-\delta_2}\,(\xi+\xi_0)\Big), \quad \xi_0 \in \mathbb{R}. \tag{4.8}$$

Family 5: When $\delta_0 > 0$, $\delta_1 = 0$, and $\delta_2 > 0$,

$$h(\xi) = \pm\sqrt{\frac{\delta_0}{\delta_2}}\,\sinh\Big(\sqrt{\delta_2}\,(\xi+\xi_0)\Big), \quad \xi_0 \in \mathbb{R}. \tag{4.9}$$

$$h(\xi) = \pm i\sqrt{\frac{\delta_0}{\delta_2}}\,\cosh\Big(\sqrt{\delta_2}\,(\xi+\xi_0)\Big), \quad \xi_0 \in \mathbb{R}. \tag{4.10}$$

Family 6: When $\delta_0 = 0$, $\delta_1 \in \mathbb{R}$, and $\delta_2 > 0$,

$$h(\xi) = \pm\frac{4\delta_2 \mathrm{e}^{-\sqrt{\delta_2}\,(\xi+\xi_0)}}{4\delta_1\delta_2 \mathrm{e}^{-2\sqrt{\delta_2}\,(\xi+\xi_0)} - 1}, \quad \xi_0 \in \mathbb{R}. \tag{4.11}$$

Family 7: When $\delta_0 = 0$, $delta_1 > 0$, and $\delta_2 > 0$,

$$h(\xi) = \pm\sqrt{\frac{\delta_2}{\delta_1}}\,\mathrm{csch}\Big(\sqrt{\delta_2}\,(\xi+\xi_0)\Big), \quad \xi_0 \in \mathbb{R}. \tag{4.12}$$

Family 8: When $\delta_0 = 0$, $\delta_1 > 0$, and $\delta_2 < 0$,

$$h(\xi) = \pm\sqrt{-\frac{\delta_2}{\delta_1}}\,\csc\Big(\sqrt{-\delta_2}\,(\xi+\xi_0)\Big), \quad \xi_0 \in \mathbb{R}. \tag{4.13}$$

$$h(\xi) = \pm\sqrt{-\frac{\delta_2}{\delta_1}}\,\sec\Big(\sqrt{-\delta_2}\,(\xi+\xi_0)\Big), \quad \xi_0 \in \mathbb{R}. \tag{4.14}$$

Family 9: When $\delta_0 = 0$, $\delta_1 < 0$, and $\delta_2 > 0$,

$$h(\xi) = \pm\sqrt{-\frac{\delta_2}{\delta_1}}\,\mathrm{sech}\Big(\sqrt{\delta_2}\,(\xi+\xi_0)\Big), \quad \xi_0 \in \mathbb{R}. \tag{4.15}$$

Family 10: When $\delta_0 = 0$, $\delta_1 > 0$, and $\delta_2 = 0$,

$$h(\xi) = \pm\frac{1}{\sqrt{\delta_1}\,(\xi+\xi_0)}, \quad \xi_0 \in \mathbb{R}. \tag{4.16}$$

Family 11: When $\delta_0 = 0$, $\delta_1\left(p^2 - q^2\right) > 0$, $p, q \in \mathbb{R}$, and $\delta_2 > 0$,

$$h(\xi) = \pm\frac{\sqrt{\delta_2\delta_1\,(p^2-q^2)}\,\mathrm{csch}\Big(\sqrt{\delta_2}\,(\xi+\xi_0)\Big)}{\delta_1\Big(p - q\coth\Big(\sqrt{\delta_2}\,(\xi+\xi_0)\Big)\Big)}, \quad \xi_0 \in \mathbb{R}. \tag{4.17}$$

Family 12: When $\delta_0 = 0$, $\delta_1 > 0$, $p, q \in \mathbb{R}$, and $\delta_2 < 0$,

$$h(\xi) = \pm\frac{\sqrt{-\delta_2\delta_1\,(p^2+q^2)}\,\csc\Big(\sqrt{-\delta_2}\,(\xi+\xi_0)\Big)}{\delta_1\Big(p - q\cot\Big(\sqrt{-\delta_2}\,(\xi+\xi_0)\Big)\Big)}, \quad \xi_0 \in \mathbb{R}. \tag{4.18}$$

$$h(\xi) = \pm \frac{\sqrt{-\delta_2\delta_1\left(p^2+q^2\right)}\,\sec\left(\sqrt{-\delta_2}\,(\xi+\xi_0)\right)}{\delta_1\left(p - q\tan\left(\sqrt{-\delta_2}\,(\xi+\xi_0)\right)\right)}, \quad \xi_0 \in \mathbb{R}. \tag{4.19}$$

Family 13: When $\delta_0 = 0$, $\delta_1\left(p^2 - q^2\right) < 0$, $p, q \in \mathbb{R}$, and $\delta_2 > 0$,

$$h(\xi) = \pm \frac{\sqrt{-\delta_2\delta_1\left(p^2-q^2\right)}\,\mathrm{sech}\left(\sqrt{\delta_2}\,(\xi+\xi_0)\right)}{\delta_1\left(p - q\tanh\left(\sqrt{\delta_2}\,(\xi+\xi_0)\right)\right)}, \quad \xi_0 \in \mathbb{R}. \tag{4.20}$$

Family 14: When $\delta_0 > 0$, $\delta_1 = 0$, and $\delta_2 = 0$,

$$h(\xi) = \pm\sqrt{\delta_0}\,(\xi+\xi_0), \quad \xi_0 \in \mathbb{R}. \tag{4.21}$$

Family 15: When $\delta_0 \in \mathbb{R}$, $\delta_1 = 1$, and $\delta_2 = 0$,

$$h(\xi) = \pm\sqrt{\wp(\xi+\xi_0, -4\delta_0, 0)}, \textit{where } \wp \textit{ is a Weierstrass function}, \quad \xi_0 \in \mathbb{R}. \tag{4.22}$$

Family 16: When $\delta_0 \in \mathbb{R}$, $\delta_1 = -1$, and $\delta_2 = 0$,

$$h(\xi) = \pm\sqrt{-\wp\,(\xi+\xi_0, 4\delta_0, 0)}, \textit{where } \wp \textit{ is a Weierstrass function}, \quad \xi_0 \in \mathbb{R}. \tag{4.23}$$

Family 17: When $\delta_0 \in \mathbb{R}$, $\delta_1 = 0$, and $\delta_2 > 0$,

$$h(\xi) = \pm\frac{1}{2\sqrt{\delta_2}}\left(\mathrm{e}^{\sqrt{\delta_2}\,(\xi+\xi_0)} - \delta_0\,\mathrm{e}^{-\sqrt{\delta_2}\,(\xi+\xi_0)}\right), \quad \xi_0 \in \mathbb{R}. \tag{4.24}$$

To clarify the mathematical diversity of the solutions, Table 1 summarizes the 17 families derived, together with their mathematical forms and the nature of solutions.

Table 1. Classification of exact solutions for the auxiliary Eq (4.1).

Families	**Mathematical forms**	**Nature of solutions**
Family 1	Jacobian elliptic	Doubly periodic waves (*sn*)
Families 2–3	Hyperbolic/Trigonometric	Solitons (tanh) and periodic (tan)
Families 4–5	Trigonometric/Hyperbolic	Linear periodic (sin) and growth (sinh)
Families 6–9	Exponential/Hyperbolic	Localized pulses and wave-fronts
Family 10	Rational function	Singular algebraic solution
Families 11–13	Combined hyperbolic	Complex soliton structures
Family 14	Polynomial	Linear growth solution
Families 15–16	Weierstrass function	Doubly periodic elliptic solutions
Family 17	Exponential difference	Kink-type behavior

Theorem 1. *Equation* (2.3) *has solutions of the following form, where* $a_0, a_1, \lambda_0, \lambda_1, \lambda_2, \mu_0$, *and* μ_1 *are real constants:*

$$\Theta(\xi) = a_0 + a_1\left(\frac{\lambda_2 h^2(\xi) + \lambda_1 h(\xi) + \lambda_0}{\mu_1 h(\xi) + \mu_0}\right). \tag{4.25}$$

Proof. The derivation process is organized as follows: First, we substitute the ansatz from Eq (4.25) and its derivatives into the nonlinear ordinary differential equation (ODE) given by (2.3). During this substitution, the derivatives of $h(\xi)$ are replaced using the auxiliary ODE (4.1) to ensure a consistent polynomial form. We then group all terms according to the powers of $h^j(\xi)$ and set each coefficient to zero, resulting in a system of nonlinear algebraic equations. This system was solved using the symbolic computation capabilities of Maple 2022. By determining the values of the parameters a_i, λ_i, and μ_i and subsequently substituting them back into Eq (4.25), we derive the sets of solutions expressed in Eqs (4.26)–(4.29). Finally, by applying the specific solution families of the auxiliary equation $h(\xi)$, we are able to construct the explicit wave structures detailed in Eqs (4.30)–(4.52).

Set 1:

$$\left\{ \begin{array}{l} a_0 = a_0,\ a_1 = a_1, \delta_0 = \delta_0,\ \delta_1 = -\frac{Ba_1^2\lambda_1^2}{2\mu_0^2},\ \delta_2 = -A, \\ \lambda_0 = -\frac{a_0\mu_0}{a_1},\ \lambda_1 = \lambda_1,\ \lambda_2 = 0, \mu_0 = \mu_0,\ \mu_1 = 0. \end{array} \right\} \tag{4.26}$$

Set 2:

$$\left\{ \begin{array}{l} a_0 = -\frac{a_1\lambda_1}{\mu_1},\ a_1 = a_1, \delta_0 = -\frac{Ba_1^2\lambda_0^2}{2\mu_1^2},\ \delta_1 = \delta_1,\ \delta_2 = -A, \\ \lambda_0 = \lambda_0,\ \lambda_1 = \lambda_1,\ \lambda_2 = 0, \mu_0 = 0,\ \mu_1 = \mu_1. \end{array} \right\} \tag{4.27}$$

Set 3:

$$\left\{ \begin{array}{l} a_0 = -\frac{a_1(\lambda_0\mu_1+\lambda_1\mu_0)}{2\mu_0\mu_1},\ a_1 = a_1, \delta_0 = -\frac{B(\lambda_1\mu_0-\lambda_0\mu_1)^2a_1^2+4A\mu_0^2\mu_1^2}{16\mu_1^4},\ \delta_1 = \frac{\mu_1^4\delta_0}{\mu_0^4}, \\ \delta_2 = \frac{-3B(\lambda_1\mu_0-\lambda_0\mu_1)^2a_1^2+4A\mu_0^2\mu_1^2}{8\mu_0^2\mu_1^2},\ \lambda_0 = \lambda_0,\ \lambda_1 = \lambda_1,\ \lambda_2 = 0, \mu_0 = \mu_0,\ \mu_1 = \mu_1. \end{array} \right\} \tag{4.28}$$

Set 4:

$$\left\{ \begin{array}{l} a_0 = a_0,\ a_1 = a_1, \delta_0 = -\frac{\mu_1^2(A+\delta_2)^2}{18Ba_1^2\lambda_2^2},\ \delta_1 = -\frac{Ba_1^2\lambda_2^2}{2\mu_1^2},\ \delta_2 = \delta_2, \\ \lambda_0 = -\frac{\mu_1^2(A+\delta_2)}{3Ba_1^2\lambda_2},\ \lambda_1 = -\frac{a_0\mu_1}{a_1},\ \lambda_2 = \lambda_2, \mu_0 = 0,\ \mu_1 = \mu_1. \end{array} \right\} \tag{4.29}$$

Using the solutions $\Theta_1(\xi), \Theta_2(\xi), \Theta_3(\xi)$, and $\Theta_4(\xi)$ obtained above, we can now determine the exact solutions of Eq (2.3). For example, utilizing Eq (4.32) together with the solutions of Eq (4.1) leads to the following solutions:

1. If $\delta_2^2 - 4\delta_0\delta_1 > 0$, and $\delta_0\delta_1 \neq 0$:

$$\Theta_{4.1}(\xi) = \left(\frac{3\lambda_2^2a_1^2B\left(\frac{\delta_0\sqrt{2}\,\mathrm{sn}\left(\frac{\sqrt{2\sqrt{\delta_2^2-4\delta_0\delta_1}-2\delta_2}}{2}(\xi+\xi_0), \frac{\sqrt{-2\left(\delta_2\sqrt{\delta_2^2-4\delta_0\delta_1}+2\delta_0\delta_1-\delta_2^2\right)\delta_0\delta_1}}{\delta_2\sqrt{\delta_2^2-4\delta_0\delta_1}+2\delta_0\delta_1-\delta_2^2} \right)}{\sqrt{\delta_0\left(\sqrt{\delta_2^2-4\delta_0\delta_1}-\delta_2\right)}} \right)^2 - (A+\delta_2)\mu_1^2}{3a_1\lambda_2\mu_1B\left(\frac{\delta_0\sqrt{2}\,\mathrm{sn}\left(\frac{\sqrt{2\sqrt{\delta_2^2-4\delta_0\delta_1}-2\delta_2}}{2}(\xi+\xi_0), \frac{\sqrt{-2\left(\delta_2\sqrt{\delta_2^2-4\delta_0\delta_1}+2\delta_0\delta_1-\delta_2^2\right)\delta_0\delta_1}}{\delta_2\sqrt{\delta_2^2-4\delta_0\delta_1}+2\delta_0\delta_1-\delta_2^2} \right)}{\sqrt{\delta_0\left(\sqrt{\delta_2^2-4\delta_0\delta_1}-\delta_2\right)}} \right)} \right). \tag{4.30}$$

2. If $\delta_2^2 - 4\delta_0\delta_1 = 0$, $\delta_1 > 0$, and $\delta_2 < 0$:

$$\Theta_{4.2}(\xi) = \left(\frac{3\lambda_2^2 a_1^2 B\left(\sqrt{-\frac{\delta_2}{2\delta_1}} \tanh\left(\sqrt{-\frac{\delta_2}{2}} (\xi + \xi_0) \right) \right)^2 - (A + \delta_2)\mu_1^2}{3a_1\lambda_2\mu_1 B \left(\sqrt{-\frac{\delta_2}{2\delta_1}} \tanh\left(\sqrt{-\frac{\delta_2}{2}} (\xi + \xi_0) \right) \right)} \right), \tag{4.31}$$

$$\Theta_{4.3}(\xi) = \left(\frac{3\lambda_2^2 a_1^2 B\left(\sqrt{-\frac{\delta_2}{2\delta_1}} \coth\left(\sqrt{-\frac{\delta_2}{2}} (\xi + \xi_0) \right) \right)^2 - (A + \delta_2)\mu_1^2}{3a_1\lambda_2\mu_1 B \left(\sqrt{-\frac{\delta_2}{2\delta_1}} \coth\left(\sqrt{-\frac{\delta_2}{2}} (\xi + \xi_0) \right) \right)} \right). \tag{4.32}$$

3. If $\delta_2^2 - 4\delta_0\delta_1 = 0$, $\delta_1 > 0$, and $\delta_2 > 0$:

$$\Theta_{4.4}(\xi) = \left(\frac{3\lambda_2^2 a_1^2 B\left(\sqrt{\frac{\delta_2}{2\delta_1}} \tan\left(\sqrt{\frac{\delta_2}{2}} (\xi + \xi_0) \right) \right)^2 - (A + \delta_2)\mu_1^2}{3a_1\lambda_2\mu_1 B \left(\sqrt{\frac{\delta_2}{2\delta_1}} \tan\left(\sqrt{\frac{\delta_2}{2}} (\xi + \xi_0) \right) \right)} \right), \tag{4.33}$$

$$\Theta_{4.5}(\xi) = \left(\frac{3\lambda_2^2 a_1^2 B\left(\sqrt{\frac{\delta_2}{2\delta_1}} \cot\left(\sqrt{\frac{\delta_2}{2}} (\xi + \xi_0) \right) \right)^2 - (A + \delta_2)\mu_1^2}{3a_1\lambda_2\mu_1 B \left(\sqrt{\frac{\delta_2}{2\delta_1}} \cot\left(\sqrt{\frac{\delta_2}{2}} (\xi + \xi_0) \right) \right)} \right). \tag{4.34}$$

4. If $\delta_0 > 0$, $\delta_1 = 0$, and $\delta_2 < 0$:

$$\Theta_{4.6}(\xi) = \left(\frac{3\lambda_2^2 a_1^2 B\left(\sqrt{-\frac{\delta_0}{\delta_2}} \sin\left(\sqrt{-\delta_2}\ (\xi + \xi_0) \right) \right)^2 - (A + \delta_2)\mu_1^2}{3a_1\lambda_2\mu_1 B \left(\sqrt{-\frac{\delta_0}{\delta_2}} \sin\left(\sqrt{-\delta_2}\ (\xi + \xi_0) \right) \right)} \right), \tag{4.35}$$

$$\Theta_{4.7}(\xi) = \left(\frac{3\lambda_2^2 a_1^2 B\left(\sqrt{-\frac{\delta_0}{\delta_2}} \cos\left(\sqrt{-\delta_2}\ (\xi + \xi_0) \right) \right)^2 - (A + \delta_2)\mu_1^2}{3a_1\lambda_2\mu_1 B \left(\sqrt{-\frac{\delta_0}{\delta_2}} \cos\left(\sqrt{-\delta_2}\ (\xi + \xi_0) \right) \right)} \right). \tag{4.36}$$

5. If $\delta_0 > 0$, $\delta_1 = 0$, and $\delta_2 > 0$:

$$\Theta_{4.8}(\xi) = \left(\frac{3\lambda_2^2 a_1^2 B\left(\sqrt{\frac{\delta_0}{\delta_2}} \sinh\left(\sqrt{\delta_2}\ (\xi + \xi_0) \right) \right)^2 - (A + \delta_2)\mu_1^2}{3a_1\lambda_2\mu_1 B \left(\sqrt{\frac{\delta_0}{\delta_2}} \sinh\left(\sqrt{\delta_2}\ (\xi + \xi_0) \right) \right)} \right). \tag{4.37}$$

6. If $\delta_0 = 0$, $\delta_1 \in \mathbb{R}$, and $\delta_2 > 0$:

$$\Theta_{4.9}(\xi) = \left(\frac{3\lambda_2^2 a_1^2 B\left(\frac{4\delta_2 e^{-\sqrt{\delta_2}(\xi+\xi_0)}}{4\delta_1\delta_2 e^{-2\sqrt{\delta_2}(\xi+\xi_0)} - 1} \right)^2 - (A + \delta_2)\mu_1^2}{3a_1\lambda_2\mu_1 B \left(\frac{4\delta_2 e^{-\sqrt{\delta_2}(\xi+\xi_0)}}{4\delta_1\delta_2 e^{-2\sqrt{\delta_2}(\xi+\xi_0)} - 1} \right)} \right). \tag{4.38}$$

7. If $\delta_0 = 0$, $\delta_1 > 0$, and $\delta_2 > 0$:

$$\Theta_{4.10}(\xi) = \left(\frac{3\lambda_2^2 a_1^2 B\left(\sqrt{\frac{\delta_2}{\delta_1}}\, \operatorname{csch}\left(\sqrt{\delta_2}\ (\xi + \xi_0)\right)\right)^2 - (A + \delta_2)\,\mu_1^2}{3a_1\lambda_2\mu_1 B\left(\sqrt{\frac{\delta_2}{\delta_1}}\, \operatorname{csch}\left(\sqrt{\delta_2}\ (\xi + \xi_0)\right)\right)} \right). \tag{4.39}$$

8. If $\delta_0 = 0$, $\delta_1 > 0$, and $\delta_2 < 0$:

$$\Theta_{4.11}(\xi) = \left(\frac{3\lambda_2^2 a_1^2 B\left(\sqrt{-\frac{\delta_2}{\delta_1}}\, \operatorname{csc}\left(\sqrt{-\delta_2}\ (\xi + \xi_0)\right)\right)^2 - (A + \delta_2)\,\mu_1^2}{3a_1\lambda_2\mu_1 B\left(\sqrt{-\frac{\delta_2}{\delta_1}}\, \operatorname{csc}\left(\sqrt{-\delta_2}\ (\xi + \xi_0)\right)\right)} \right), \tag{4.40}$$

$$\Theta_{4.12}(\xi) = \left(\frac{3\lambda_2^2 a_1^2 B\left(\sqrt{-\frac{\delta_2}{\delta_1}}\, \sec\left(\sqrt{-\delta_2}\ (\xi + \xi_0)\right)\right)^2 - (A + \delta_2)\,\mu_1^2}{3a_1\lambda_2\mu_1 B\left(\sqrt{-\frac{\delta_2}{\delta_1}}\, \sec\left(\sqrt{-\delta_2}\ (\xi + \xi_0)\right)\right)} \right). \tag{4.41}$$

9. If $\delta_0 = 0$, $\delta_1 < 0$, and $\delta_2 > 0$:

$$\Theta_{4.13}(\xi) = \left(\frac{3\lambda_2^2 a_1^2 B\left(\sqrt{-\frac{\delta_2}{\delta_1}}\, \operatorname{sech}\left(\sqrt{\delta_2}\ (\xi + \xi_0)\right)\right)^2 - (A + \delta_2)\,\mu_1^2}{3a_1\lambda_2\mu_1 B\left(\sqrt{-\frac{\delta_2}{\delta_1}}\, \operatorname{sech}\left(\sqrt{\delta_2}\ (\xi + \xi_0)\right)\right)} \right). \tag{4.42}$$

10. If $\delta_0 = 0$, $\delta_1 > 0$, and $\delta_2 = 0$:

$$\Theta_{4.14}(\xi) = \left(\frac{3\lambda_2^2 a_1^2 B\left(\frac{1}{\sqrt{\delta_1}\,(\xi+\xi_0)}\right)^2 - A\mu_1^2}{3a_1\lambda_2\mu_1 B\left(\frac{1}{\sqrt{\delta_1}\,(\xi+\xi_0)}\right)} \right). \tag{4.43}$$

11. If $\delta_0 = 0$, $\delta_1\left(p^2 - q^2\right) > 0$, and $\delta_2 > 0$:

$$\Theta_{4.15}(\xi) = \left(\frac{3\lambda_2^2 a_1^2 B\left(\frac{\sqrt{\delta_2\delta_1\left(p^2-q^2\right)}\operatorname{csch}\left(\sqrt{\delta_2}\,(\xi+\xi_0)\right)}{\delta_1\left(p-q\coth\left(\sqrt{\delta_2}\,(\xi+\xi_0)\right)\right)}\right)^2 - (A + \delta_2)\,\mu_1^2}{3a_1\lambda_2\mu_1 B\left(\frac{\sqrt{\delta_2\delta_1\left(p^2-q^2\right)}\operatorname{csch}\left(\sqrt{\delta_2}\,(\xi+\xi_0)\right)}{\delta_1\left(p-q\coth\left(\sqrt{\delta_2}\,(\xi+\xi_0)\right)\right)}\right)} \right). \tag{4.44}$$

12. If $\delta_0 = 0$, $\delta_1 > 0$, and $\delta_2 < 0$:

$$\Theta_{4.16}(\xi) = \left(\frac{3\lambda_2^2 a_1^2 B\left(\frac{\sqrt{-\delta_2\delta_1\left(p^2+q^2\right)}\,\csc\left(\sqrt{-\delta_2}\,(\xi+\xi_0)\right)}{\delta_1\left(p-q\cot\left(\sqrt{-\delta_2}\,(\xi+\xi_0)\right)\right)}\right)^2 - (A + \delta_2)\,\mu_1^2}{3a_1\lambda_2\mu_1 B\left(\frac{\sqrt{-\delta_2\delta_1\left(p^2+q^2\right)}\,\csc\left(\sqrt{-\delta_2}\,(\xi+\xi_0)\right)}{\delta_1\left(p-q\cot\left(\sqrt{-\delta_2}\,(\xi+\xi_0)\right)\right)}\right)} \right), \tag{4.45}$$

$$\Theta_{4.17}(\xi) = \left(\frac{3\lambda_2^2 a_1^2 B\left(\frac{\sqrt{-\delta_2\delta_1\left(p^2+q^2\right)}\,\sec\left(\sqrt{-\delta_2}\,(\xi+\xi_0)\right)}{\delta_1\left(p-q\tan\left(\sqrt{-\delta_2}\,(\xi+\xi_0)\right)\right)}\right)^2 - (A + \delta_2)\,\mu_1^2}{3a_1\lambda_2\mu_1 B\left(\frac{\sqrt{-\delta_2\delta_1\left(p^2+q^2\right)}\,\sec\left(\sqrt{-\delta_2}\,(\xi+\xi_0)\right)}{\delta_1\left(p-q\tan\left(\sqrt{-\delta_2}\,(\xi+\xi_0)\right)\right)}\right)} \right). \tag{4.46}$$

13. If $\delta_0 = 0$, $\delta_1\left(b^2 - c^2\right) < 0$, and $\delta_2 > 0$:

$$\Theta_{4.18}(\xi) = \left(\frac{3\lambda_2^2 a_1^2 B\left(\frac{\sqrt{-\delta_2\delta_1\left(p^2-q^2\right)}\,\mathrm{sech}\left(\sqrt{\delta_2}\,(\xi+\xi_0)\right)}{\delta_1\left(p-q\tanh\left(\sqrt{\delta_2}\,(\xi+\xi_0)\right)\right)} \right)^2 - (A+\delta_2)\,\mu_1^2}{3a_1\lambda_2\mu_1 B\left(\frac{\sqrt{-\delta_2\delta_1\left(p^2-q^2\right)}\,\mathrm{sech}\left(\sqrt{\delta_2}\,(\xi+\xi_0)\right)}{\delta_1\left(p-q\tanh\left(\sqrt{\delta_2}\,(\xi+\xi_0)\right)\right)} \right)} \right). \tag{4.47}$$

14. If $\delta_0 > 0$, $\delta_1 = 0$, and $\delta_2 = 0$:

$$\Theta_{4.19}(\xi) = \left(\frac{3\lambda_2^2 a_1^2 B\left(\sqrt{\delta_0}\,(\xi+\xi_0)\right)^2 - A\mu_1^2}{3a_1\lambda_2\mu_1 B\left(\sqrt{\delta_0}\,(\xi+\xi_0)\right)} \right). \tag{4.48}$$

15. If $\delta_0 \in \mathbb{R}$, $\delta_1 = 1$, and $\delta_2 = 0$:

$$\Theta_{4.20}(\xi) = \left(\frac{3\lambda_2^2 a_1^2 B\left(\sqrt{\wp(\xi+\xi_0,-4\delta_0,0)}\right)^2 - A\mu_1^2}{3a_1\lambda_2\mu_1 B\left(\sqrt{\wp(\xi+\xi_0,-4\delta_0,0)}\right)} \right). \tag{4.49}$$

16. If $\delta_0 \in \mathbb{R}$, $\delta_1 = -1$, and $\delta_2 = 0$:

$$\Theta_{4.21}(\xi) = \left(\frac{3\lambda_2^2 a_1^2 B\left(\sqrt{-\wp\,(\xi+\xi_0,4\delta_0,0)}\right)^2 - A\mu_1^2}{3a_1\lambda_2\mu_1 B\left(\sqrt{-\wp\,(\xi+\xi_0,4\delta_0,0)}\right)} \right). \tag{4.50}$$

17. If $\delta_0 \in \mathbb{R}$, $\delta_1 = 0$, and $\delta_2 > 0$:

$$\Theta_{4.22}(\xi) = \left(\frac{3\lambda_2^2 a_1^2 B\left(\frac{1}{2\sqrt{\delta_2}}\left(\mathrm{e}^{\sqrt{\delta_2}\,(\xi+\xi_0)} - \delta_0\,\mathrm{e}^{-\sqrt{\delta_2}\,(\xi+\xi_0)}\right)\right)^2 - (A+\delta_2)\,\mu_1^2}{3a_1\lambda_2\mu_1 B\left(\frac{1}{2\sqrt{\delta_2}}\left(\mathrm{e}^{\sqrt{\delta_2}\,(\xi+\xi_0)} - \delta_0\,\mathrm{e}^{-\sqrt{\delta_2}\,(\xi+\xi_0)}\right)\right)} \right). \tag{4.51}$$

Substituting the solutions $\Theta_{4.l}(\xi)$ $(l = 1, 2, \ldots, 22)$ into Eq (2.2) and using the relation $R = \varepsilon\,\overline{\Xi}$ leads to the following solutions of the Kuralay-II equation:

$$\begin{cases} \Xi_{4.l}(x,t) = \Theta_{4.l}(\xi)e^{i\kappa}, \\ \Lambda_{4.l}(x,t) = \frac{2\varepsilon m_2}{(1-m_1)}\Theta_{4.l}^2(\xi) + c, \\ R_{4.l}(\xi) = \varepsilon\overline{\Xi_{4.l}\,(\xi)},\ l = 1, 2, \ldots, 22, \end{cases} \tag{4.52}$$

where $\kappa = m_1 x + m_2 t, c = c_1 m_2/k_1(1-m_1), \xi = (k_1(1-m_1)/m_2)x + k_1 t, m_1 \notin \{0,1\}, m_2 \neq 0$, and $k_1 \neq 0$. □

5. Graphical representations and discussions

This section examines particular solutions of the Kuralay-II equation obtained from Set 4. We present three-dimensional graphical representations of the absolute value and real part, which illustrate

how these solutions behave as parameter values change. We begin by exploring the function $\Xi_{4.2}(\xi)$ obtained by substituting $\delta_2 = -1, m_1 = 2, m_2 = 10, a_1 = 11, \mu_1 = 1, \mu_0 = 0, k_1 = 5, \lambda_2 = 11, \epsilon = -1$, and $c = -30$ into $\Theta_{4.2}(\xi)$, followed by the application of Eq (4.52). Figure 10 shows the real and absolute components, where $\xi = -1/2x + 5t$, and $\xi_0 = 1$. This visualization reveals a linearly growing traveling wave solution within the domains $-\pi/8 < x < \pi/8$ and $-\pi/8 < t < \pi/8$.

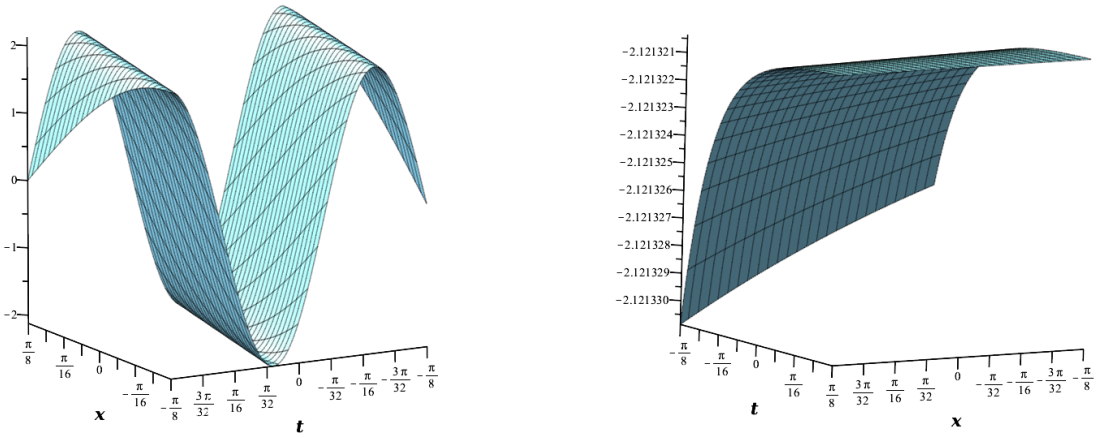

(a) Real part (b) Absolute part

Figure 10. The real and absolute parts of $\Xi_{4.2}(x, t)$ within the domains $-\pi/8 < x < \pi/8$ and $-\pi/8 < t < \pi/8$.

Figure 11 presents the real and absolute parts of the function $\Xi_{4.4}(\xi)$, where $\xi = -10x + 5t$, and $\xi_0 = 1$. The function results from substituting $\delta_2 = 1/10, m_1 = 3, m_2 = 1, a_1 = 1, \mu_1 = 2, \mu_0 = 0, k_1 = 5, \lambda_2 = 1, \epsilon = -1$, and $c = 22$ into $\Theta_{4.4}(\xi)$ and applying Eq (4.52). The figure illustrates a singular periodic soliton wave profile in the domains $-\pi/2 < x < \pi/2$ and $-\pi/2 < t < \pi/2$.

Figure 12 shows the real and absolute values of the function $\Xi_{4.5}(\xi)$, where $\xi = -1/2x + 5t$, and $\xi_0 = 1$. The function is obtained by substituting $\delta_2 = 8, m_1 = 2, m_2 = 10, a_1 = 11, \mu_1 = 1, \mu_0 = 0, k_1 = 5, \lambda_2 = 11, \epsilon = -1$, and $c = -30$ into $\Theta_{4.5}(\xi)$, followed by the application of Eq (4.52). The figure illustrates a singular periodic soliton wave in its real and absolute values within the domains $-\pi/8 < x < \pi/8$ and $-\pi/8 < t < \pi/8$.

Finally, we present the function $\Xi_{4.11}(\xi)$ where $\xi = -2x + 5t$, and $\xi_0 = 1$. This function results from substituting $\delta_2 = 6/5$, $m_1 = 3$, $m_2 = 5$, $a_1 = 1$, $\mu_1 = 2$, $\mu_0 = 0$, $k_1 = 5$, $\lambda_2 = 1$, $\epsilon = -1$, and $c = 22$ into $\Theta_{4.10}(\xi)$, followed by the application of Eq (4.52). Figure 13(b) displays a singular kink profile, and Figure 13 illustrates soliton shapes within the domains $-\pi < x < \pi$ and $-\pi < t < \pi$.

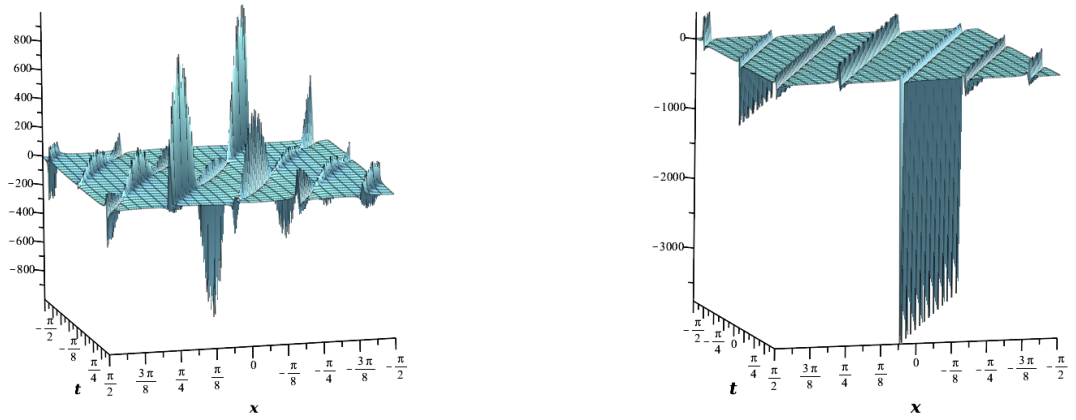

(a) Real part (b) Absolute part

Figure 11. The real and absolute parts of $\Xi_{4.4}(x,t)$ within the domains $-\pi/2 < x < \pi/2$ and $-\pi/2 < t < \pi/2$.

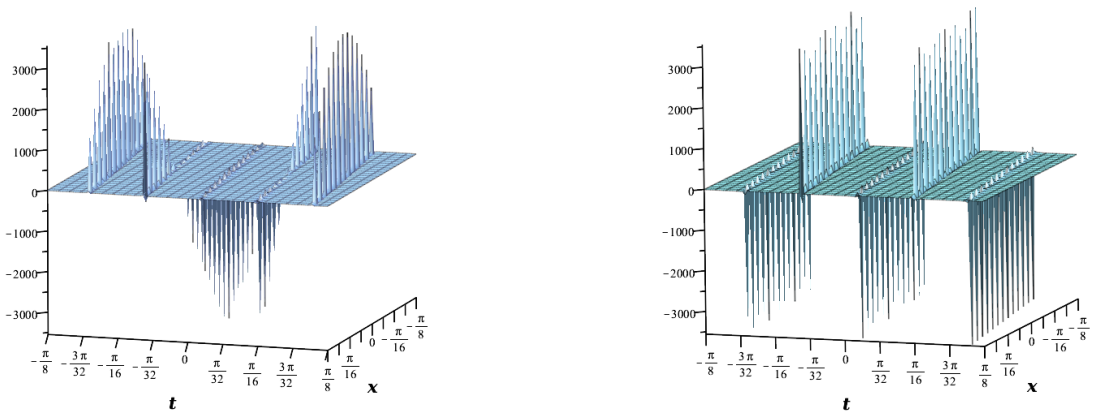

(a) Real part (b) Absolute part

Figure 12. The real and absolute parts of $\Xi_{4.5}(x,t)$ within the domain $-\pi/8 < x < \pi/8$ and $-\pi/8 < t < \pi/8$.

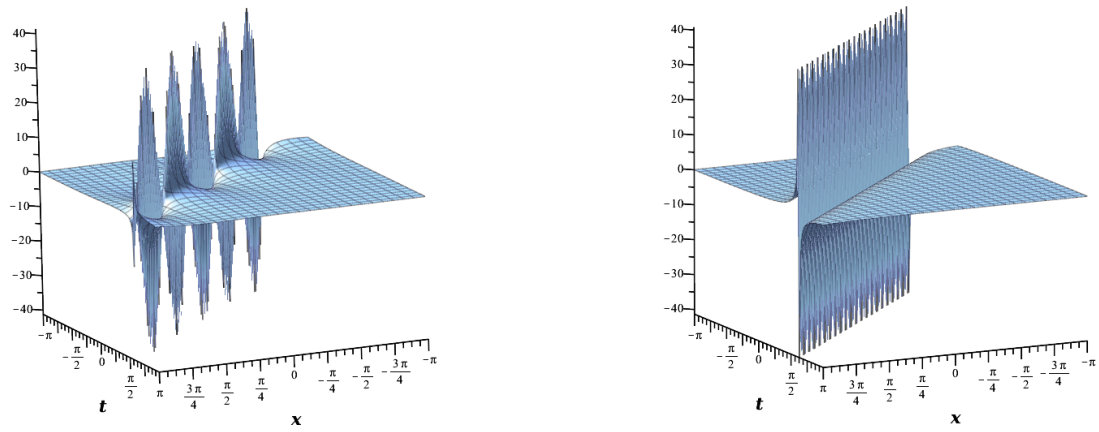

(a) Real part (b) Absolute part

Figure 13. The real and absolute parts of $\Xi_{4.10}(x,t)$ within the domains $-\pi < x < \pi$ and $-\pi < t < \pi$.

6. Physical analysis and comparative study

This section analyzes the physical characteristics of the derived solutions $\Xi_{4.1}$–$\Xi_{4.11}$ and compares them with those in the existing literature. The current method reveals a broader range of behaviors and diverse wave structures, as illustrated in Figures 10–13. Specifically, this method can identify amplifying pulse envelopes (Figure 10), singular rogue-wave precursors (Figure 11), nonlinear resonance oscillations (Figure 12), and singular kink profiles that represent topological defects (Figure 13).

A comparative assessment with the approaches proposed in [20, 24, 26, 27] shows that our results encompass all the solutions presented in these studies. Specifically, our method reproduces the standard bright and dark solitons reported in [20, 24]. However, our singular periodic structures ($\Xi_{4.4}, \Xi_{4.5}$) and the csch-based localized solutions were not documented in [20, 24]. Additionally, our findings are consistent with the Jacobi elliptic solutions in [26], and the kink profile in $\Xi_{4.11}$ generalizes the topological solitons identified in [27]. Overall, our framework not only confirms known wave types but also expands the solution landscape of the Kuralay-II equation by introducing novel singular and kink-type structures.

7. Conclusions

In this work, we conducted a comprehensive investigation into the dynamics of the Kuralay-II equation. Starting with an analysis of its bifurcation structure and phase portraits, we gained insights into the dynamical transitions of the system. We then used Lyapunov stability analysis to assess the presence of chaos and quantify the sensitivity to initial conditions. In addition, we derived multiple

exact solutions using a direct analytical method and visualized the absolute and real parts of some selected solutions to emphasize their structural complexity and physical relevance. These findings enhance our understanding of nonlinear models and underscore their potential applications in diverse scientific and engineering fields. Future research could enhance the proposed framework by examining the Kuralay-II equation in higher dimensions, including (2 + 1) or (3 + 1), which would allow for the exploration of more complex localized structures. Additionally, a comparative analysis with existing methods should be conducted, particularly focusing on the quantity and nature of the solutions obtained. Investigating the effects of stochastic perturbations or time-fractional derivatives on chaotic transitions would also yield valuable insights into real-world applications in nonlinear optics. Finally, the use of machine learning techniques to predict soliton stability in the presence of noise represents a promising avenue for future exploration.

Author contributions

A.M.: Writing original draft, software, methodology, editing; L.A.: Writing original draft, software, methodology, validation; A.S.: Writing original draft, software; Y.M.: supervision, editing; B.G.: Writing original draft, software, methodology, editing. All authors have read and approved the final version of the manuscript for publication.

Use of Generative-AI tools declaration

The authors declare they have not used Artificial Intelligence (AI) tools in the creation of this article.

Acknowledgments

The Researchers would like to thank the Deanship of Graduate Studies and Scientific Research at Qassim University for financial support (QU-APC-2026).

Conflict of interest

The authors declare that they have no known competing financial interests or personal relationships that could have appeared to influence the work reported in this paper.

References

1. C. V. Archana, R. S. Twinkle, Mathematical modeling of tsunami wave propagation at mid ocean and its amplification and run-up on shore, *J. Ocean Eng. Sci.*, **6** (2021), 367–375. https://doi.org/10.1016/j.joes.2021.03.003
2. B. Gasmi, A. Moussa, Y. Mati, L. Alhakim, A. Akgül, Solving nonlinear partial differential equations using a novel Cham method, *J. Taibah Univ. Sci.*, **17** (2023), 2272728. https://doi.org/10.1080/16583655.2023.2272728

3. B. Gasmi, L. Alhakim, Y. Mati, A. Moussa, H. M. Baskonus, New analytical solutions to the nonlinear Schrödinger equation via an improved Cham method in conformable operator, *Mod. Phys. Lett. B*, **38** (2024), 2450327. https://dx.doi.org/10.1142/S0217984924503275
4. M. A. Bashir, A. A. Moussa, The $\coth_a(\xi)$ expansion method and its application to the Davey–Stewartson equation, *Appl. Math. Sci.*, **8** (2014), 3851–3868. http://dx.doi.org/10.12988/ams.2014.45362
5. B. Gasmi, A. A. Moussa, Y. Mati, L. A. Alhakim, A. Akgül, New exact traveling wave solutions to the Kawahara equation using the $\tanh(\xi)$ expansion method, *Int. J. Appl. Comput. Math.*, **9** (2023), 98. https://doi.org/10.1007/s40819-023-01568-6
6. W. B. Rabie, M. M. Ahmed, M. Marin, M. F. Ismail, Exact wave solutions for rotational effects in temperature-dependent thermoelastic materials via IMETF technique, *IJST-T. Mech. Eng.*, **50** (2026), 1–28. https://doi.org/10.1007/s40997-025-00917-8
7. M. A. Bashir, A. A. Moussa, New approach of $\left(\frac{G'}{G}\right)$ expansion method. applications to KdV equation, *J. Math. Res.*, **6** (2014), 24–32. http://dx.doi.org/10.5539/jmr.v6n1p24
8. M. S. Jazmati, Analytical solutions of some nonlinear space-time fractional differential equations via improved exp-function method, *J. Nat. Sci. Math.*, **9** (2016), 1–16.
9. L. A. Alhakim, A. A. Moussa, The double auxiliary equations method and its application to space-time fractional nonlinear equations, *J. Ocean Eng. Sci.*, **4** (2019), 7–13. https://doi.org/10.1016/j.joes.2018.12.002
10. B. Gasmi, A. Moussa, Y. Mati, L. Alhakim, H. M. Baskonus, Bifurcation and exact traveling wave solutions to a conformable nonlinear Schrödinger equation using a generalized double auxiliary equation method, *Opt. Quant. Electron.*, **56** (2024), 18. http://dx.doi.org/10.1007/s11082-023-05578-y
11. W. B. Rabie, H. B. Amer, H. Khan, J. Alzabut, D. I. Elimy, Exact solutions and stability thresholds for the fractional gardner equation with high-order dispersion, *Eur. J. Pure Appl. Math.*, **19** (2026), 6805–6805. https://doi.org/10.29020/nybg.ejpam.v19i1.6805
12. W. B. Rabie, H. M. Ahmed, M. E. Ramadan, N. S. E. Abdalla, A. Abd-Elmonem, T. A. Sulaiman, et al., Dual-soliton structures and stability analysis in a nonlinear fractional Schrodinger equation with dual-mode dispersion using modified extended mapping method, *Mod. Phys. Lett. A*, 2026. https://doi.org/10.1142/S021773232650077X
13. N. Das, S. S. Ray, Investigations of bright, dark, kink-antikink optical and other soliton solutions and modulation instability analysis for the (1+1)-dimensional resonant nonlinear Schrödinger equation with dual-power law nonlinearity, *Opt. Quant. Electron.*, **55** (2023), 1071. http://dx.doi.org/10.1007/s11082-023-05341-3
14. K. J. Wang, F. Shi, Multi-soliton solutions and soliton molecules of the (2+1)-dimensional Boiti-Leon-Manna-Pempinelli equation for the incompressible fluid, *Europhysics Lett.*, **145** (2024), 42001. https://doi.org/10.1209/0295-5075/ad219d
15. A. M. Alqahtani, S. Akram, M. Alosaimi, Study of bifurcations, chaotic structures with sensitivity analysis and novel soliton solutions of non-linear dynamical model, *J. Taibah Univ. Sci.*, **18** (2024), 2399870. https://doi.org/10.1080/16583655.2024.2399870

16. S. A. El-Tantawy, H. A. Alyousef, R. T. Matoog, R. Shah, On the optical soliton solutions to the fractional complex structured (1+1)-dimensional perturbed gerdjikov-ivanov equation, *Phys. Scripta*, **99** (2024), 035249. https://doi.org/10.1088/1402-4896/ad241b

17. J. Zhang, G. Wang, Similarity transformations and exact solutions of the (3+1)-dimensional nonlinear Schrödinger equation with spatiotemporally varying coefficients, *Appl. Math. Lett.*, **159** (2025), 109286. https://doi.org/10.1016/j.aml.2024.109286

18. S. Hajiollow, F. Zabihi, Using the spectral meshless radial basis functions method for solving time fractional Burgers' equation, *Bound. Value Probl.*, **2025** (2025). https://doi.org/10.1186/s13661-025-02075-x

19. H. Riaz, A. Wajahat, Exact multisolitons of noncommutative and commutative Lakshmanan–Porsezian–Daniel equation, *Eur. Phys. J. Plus*, **135** (2020), 508. https://doi.org/10.1140/epjp/s13360-020-00505-6

20. T. Mathanaranjan, Optical soliton, linear stability analysis and conservation laws via multipliers to the integrable Kuralay equation, *Optik*, **290** (2023), 171266. https://doi.org/10.1016/j.ijleo.2023.171266

21. M. Iqbal, D. Lu, A. R. Seadawy, N. E. Alsubaie, Z. Umurzakhova, R. Myrzakulov, Dynamical analysis of exact optical soliton structures of the complex nonlinear Kuralay-II equation through computational simulation, *Mod. Phys. Lett. B*, **38** (2024), 2450367. https://dx.doi.org/10.1142/S0217984924503676

22. Z. Sagidullayeva, G. Nugmanova, R. Myrzakulov, N. Serikbayev, Integrable Kuralay equations: Geometry, solutions and generalizations, *Symmetry*, **14** (2022), 1374. https://doi.org/10.3390/sym14071374

23. Y. Meng, H. W. A. Riaz, J. Lin, New types of nondegenerate solitons for a (2+1)-dimensional coupled system, *Commun. Theor. Phys.*, **77** (2025), p095001. https://doi.org/10.1088/1572-9494/adc240

24. S. Y. Arafat, S. R. Islam, Bifurcation analysis and soliton structures of the truncated M-fractional Kuralay-II equation with two analytical techniques, *Alex. Eng. J.*, **105** (2024), 70–87. https://doi.org/10.1016/j.aej.2024.06.079

25. A. Zafar, M. Raheel, M. R. Ali, Z. Myrzakulova, A. Bekir, R. Myrzakulov, Exact solutions of m-fractional Kuralay equation via three analytical schemes, *Symmetry*, **15** (2023), 1862. https://doi.org/10.3390/sym15101862

26. A. Farooq, W. X. Ma, M. I. Khan, Exploring exact solitary wave solutions of Kuralay-II equation based on the truncated M-fractional derivative using the Jacobi Elliptic function expansion method, *Opt. Quant. Electron.*, **56** (2024), 1105. https://doi.org/10.1007/s11082-024-06841-6

27. W. A. Faridi, M. A. Bakar, Z. Myrzakulova, R. Myrzakulov, A. Akgül, S. M. El Din, The formation of solitary wave solutions and their propagation for Kuralay equation, *Results Phys.*, **52** (2023), 106774. https://doi.org/10.1016/j.rinp.2023.106774

28. V. F. Marcelo, P. Efim, Interactions of solitons with an external force field: Exploring the Schamel equation framework, *Chaos Soliton. Fract.*, **174** (2023), 113799. https://doi.org/10.13140/RG.2.2.20039.98726

29. J. Zhang, Z. Zheng, H. Meng, Z. Wang, Bifurcation analysis and exact solutions of the conformable time fractional Symmetric Regularized Long Wave equation, *Chaos Soliton. Fract.*, **190** (2025), 115744. https://doi.org/10.1016/j.chaos.2024.115744

30. A. H. Arnous, Chaotic dynamics and bifurcation analysis of optical solitons in birefringent fibers governed by the Sasa-Satsuma equation with stochastic perturbation, *Nonlinear Dyn.*, **113** (2025), 18469–18484. https://doi.org/10.1007/s11071-025-11107-1

31. I. Melnikov, M. V. Flamarion, Soliton dynamics under the influence of an external force and induced-damped terms within the modified Korteweg-de Vries equation, *Nonlinear Dyn.*, 2026. https://doi.org/10.1007/s11071-025-11963-x

32. Z. Hua, Z. Wu, Y. Zhang, H. Bao, Y. Zhou, Two-dimensional cyclic chaotic system for noise-reduced OFDM-DCSK communication, *IEEE T. Circuits-I*, **72** (2024), 323–336. https://doi.org/10.1109/TCSI.2024.3454535

33. R. M. Mamunur, Exploring the chaotic behavior, and ion acoustic wave of generalized perturbed Korteweg-de Vries equation with a fractional operator, *Part. Diff. Equ. Appl. Math.*, **13** (2025). https://doi.org/10.1016/j.padiff.2024.101042

AIMS Press

© 2026 the Author(s), licensee AIMS Press. This is an open access article distributed under the terms of the Creative Commons Attribution License (https://creativecommons.org/licenses/by/4.0)